Response to RC1

The authors have done a great effort to answer all reviewer comments appropriately. This manuscript has significantly improved as a result. The writing style however can still be considered somewhat sloppy at some instances. Technical corrections are therefore suggested below, but the authors are encouraged to have the final version of their manuscript revised by a native English speaker.

Lines 30-33: Rewrite for clarity. Statistical analysis of what? Start a new sentence afterwards: "The grid box size was also..."

done

Line 35: "coordinated by the European Commission"

Done

Line 48: "contributing missions" is unclear here. What is contributing to what? Other missions contributing to the Sentinels would be misleading...

Removed

Line 49: "encompass from" is a wrong wording.

Replaced with include

Line 53: "The three approaches differ…"

done

Line 60: Two times particular(ly).

Removed particularly.

Line 65: Mismatch between single and plural.

corrected

Line 65: "which collects all the available information content" sounds vague. Something like "which optimizes the DFS of the fused product" and including a reference to one of the technical papers?

… in which the sensitivity increases and the error reduces (Ceccherini et al., 2015).

Line 70: "the algorithm" – which one is intended here; or should this be plural, referring to all previously mentioned?

Should be plural, even if in this article we consider only the first

Line 77: "and discuss the use of the profiles average as fusion technique" - This addition is misleading, as if averaging is the main fusion technique. Suggestion: "and discuss the differences between CDF and mere averaging"

done

Lines 89-91: Duplication of following?

89-91 represent a general description, in the following more detailed description is presented.

Line 149: "specifications used for the simulation"

"in" was removed

Line 159: “Eqs.”

done

Line 163: “Concerning the profile and the error the CDF…”

done

Lines 169-171: Could you briefly elaborate on how this 5% choice is made based on grid cell size? How should other users of the CDF method make such decisions for different grids? Could you provide a few references?

The 5% choice matured in a heuristic way by varying its value and observing the quality of the fused product, both for some single cells chosen as a reference and by looking at the Synergy Factors of the entire dataset using similar representations to figures 6 and 7 (added in the text, lines 178-180).

The figure below (not in the paper) refers to the cell of figures 1-4, representing FUS total error profile, the L2 total error average profile, the 5% of the a priori profile and the standard deviation profile of the "virtual truth" in the cell of interest. Note here that the black error profile is about half of the green one and in any case always larger than the blue one at all heights. This is a confirmation of the following sentence in the paper (lines 184-186) : “… even if the coincidence error is strictly needed for the correct behaviour of the CDF product, this is not strongly dependant by its exact amount until it is smaller with respect to the errors of the individual L2 products”. In the same paragraph we cite (Ceccherini et al. 2019) both to justify the heuristic approach (see above) and to suggest an alternative recipe to the $\mathbf{S}_{\mathbf{coinc}}$ choice.

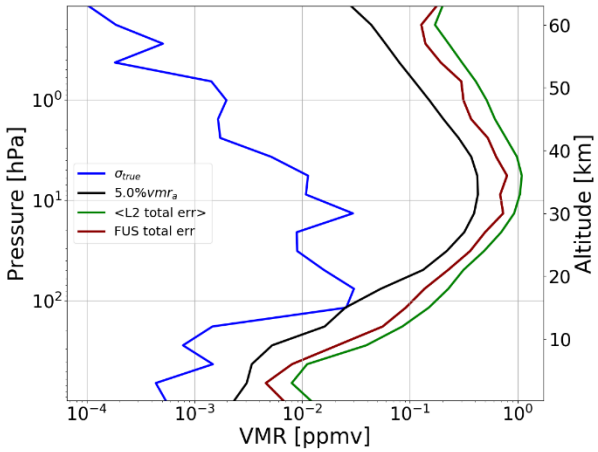

Eq. (8): Remove “= …”

done

Lines 208-209: “used in this article”

done

Line 231: “allows seeing”

done

Line 249: Remove “as suggested by one of the reviewers”

removed

Line 254: Replace “contribute of the measures” by something like “contribution of the (simulated) measurements”

Replaced

Response to RC2

The manuscript by Zoppetti et al. has improved in clarity for some of the aspects remarked by the reviewers. However, major revisions are still needed, and the manuscript cannot be published in the current state. My major concern is that there are mistakes in the characteristics of the instruments onboard MTG-S and EPS-SG together with the instruments Sentinel 4 and 5, whose measurements are simulated for demonstrating the performance of the Fusion algorithm. These instrumental characteristics are greatly important in this work. They must be corrected and all the results using these simulated measurements (Figures 3, 4, 6 and 7) should be done again with the correct configuration.

Thanks to the reviewer's comments, we realized that there is a fundamental misunderstanding about the L2 simulated products characteristics and more in general on the paper objectives. Moreover, we realized that the specifications of the considered platform significantly changed from the one considered for simulations. In fact, we simulated L2 products in the context of an H2020 project that started in 2016 and ended in 2019 were the simulation was one of the first steps. The primary references for all the simulated products were the documents listed below, dated between 2007 and 2012.

- [D4] Jörg Langen, European Space Agency (ESA), (2007) GMES Sentinels 4 and 5 Mission Requirements Traceability Document (MRTD), EOP-SMA/1507/JL-dr, issue 1 rev.0. https://earth.esa.int/web/guest/document-library/browse-document-library/-/article/gmes-sentinels-4-and-5-mission-requirements-document-6442
- [D42] Mission Science Division, European Space Agency (ESA), (2012) GMES Sentinels 4 and 5 Mission Requirements Traceability Document (MRTD), EOP-SM/2413/BV-bv, issue 1 rev.0. http://aurora.ifac.cnr.it/utils/personaldocs/see/96/
- [D5] EUMETSAT, (2010) MTG End-User Requirements Document [EURD], EUM/MTG/SPE/07/0036, v3C https://www.ncdc.noaa.gov/sites/default/files/attachments/PDF_MTG_EURD.pdf
- [D6] European Space Agency (ESA), (2012) GMES Sentinels 4 and 5 Mission Requirements Document (MRD), EOP-SM/2413, issue 1 rev.0. http://aurora.ifac.cnr.it/utils/personaldocs/see/93/
- Crevoisier, C., Clerbaux, C., Guidard, V., Phulpin, T., Armante, R., Barret, B., Camy-Peyret, C., Chaboureau, J.-P., Coheur, P.-F., Crépeau, L., Dufour, G., Labonnote, L., Lavanant, L., Hadji-Lazaro, J., Herbin, H., Jacquinet-Husson, N., Payan, S., Péquignot, E., Pierangelo, C., Sellitto, P., and Stubenrauch, C.: Towards IASI-New Generation (IASI-NG): impact of improved spectral resolution and radiometric noise on the retrieval of thermodynamic, chemistry and climate variables, Atmos. Meas. Tech., 7, 4367–4385, https://doi.org/10.5194/amt-7-4367-2014, 2014.

The result is a set of L2 products that do not follow the updated specifications of the considered platforms. Since the project ended in 2019, it is not possible to repeat now the L2 product characterization and simulation process, as requested by the reviewer.

Nevertheless, this work focuses on a relative comparison of the fused and L2 products and on the ability of the Complete Data Fusion inducing quality improvements that are, in some sense, independent from precise instrumental characteristics.

On the other hand, we realize that these considerations have to be clearly stated in the introduction (paragraph added, lines 80-86) so that the reader can concentrate her/his attention on the more relevant aspect of this study.

In this sense, it is also opportune to change (again) the title of the article in "APPLICATION OF THE COMPLETE DATA FUSION TO THE OZONE PROFILES MEASURED BY GEOSTATIONARY AND LOW EARTH ORBITS SATELLITES: A FEASIBILITY STUDY".

In the following, we will answer to the other points raised by the reviewer using as reference the already cited documents and also the Requirements Document and the Technical Note cited below.

- [D2.1] AURORA consortium, (Advanced Ultraviolet Radiation and Ozone Retrieval For Applications, grant no. 687428): Requirements document Issue: 1, rev. 4 Date: 31-Mar-2016 http://aurora.ifac.cnr.it/utils/personaldocs/see/97/
- [D3.4] AURORA consortium, (Advanced Ultraviolet Radiation and Ozone Retrieval For Applications, grant no. 687428): Technical Note On L2 Data Simulations, 35 pp. http://aurora.ifac.cnr.it/utils/personaldocs/see/95/

IRS onboard MTG-S (called in the paper S4-TIR): this sensor is NOT IASI-NG (nor IRS2b) which is described by Crevoisier et al. (2014). Crevoisier et al. (2014) do NOT describe the instrument that will be onboard the geostationary satellite MTG-S together with UVN/Sentinel 4, but they only describe IASI-NG which will be onboard the low orbit EPS-SG satellite together with Sentinel 5/UVNS. IASI-NG is supposed to be S5-TIR in the paper. EUMETSAT describes IRS onboard MTG-S here: https://www.eumetsat.int/website/home/Satellites/FutureSatellites/MeteosatThirdGeneration/MTGDesign/index.html "The Infrared Sounder (IRS) on MTG-S … with a hyperspectral resolution of 0.625 cm-1 wave-number..." This means that IRS onboard MTG-S (in your paper S4-TIR) will have an even coarser spectral resolution than IASI (0.5 cm-1) and much coarser resolution than IASI-NG (0.25 cm-1). The SNR for IRS onboard MTG-S will be much lower than that for IASI-NG and similar to IASI. IASI, with a finer spectral resolution than IRS/MTG-S, enables the retrieval of ozone with 3,5 DOFs at most. Therefore, it is not possible to obtain 5 degrees of freedom for the retrieval of the ozone total column derived from IRS onboard MTG-S, as illustrated in Figure 3 of the paper. In consequence, all simulations and retrievals using S4-TIR must be done again with the correct instrumental characteristics of this instrument. Figures 3, 4, 6 and 7 should be revised with correct simulations of IRS/MTG-S measurements.

S4-TIR products are simulated according to [D4], [D42] and [D6] and their characteristics are summarized in [D3.4] from which we extracted the following table 8. In particular the NESR value of table 8 derived from (Crevoisier et al. 2014, IRS1b scenario). With these characteristics, the 5 degrees of freedom can be due to both the small error adopted and the relatively low a priori strength compared to operational retrieval conditions. As already said in the previous paragraph, it is not possible to repeat the simulations, and we also think that it is not worth to do. In this paper, we want to show the feasibility and the potential benefits of the a-posteriori fusion approach, and we think that the goal is reached even without an exact instrument characterization. Since we believe in achieving this objective, the next step of this research activity will be applying CDF to real data.

	Description
Instrument	Infrared Sounder (IRS)
O_3 retrieval spectral range (cm^{-1})	1030-1080
Spectral resolution (cm^{-1})	0.625 (apodized IRSF)
Spectral sampling (cm^{-1})	0.625
NESR	IASI L1C VCM/4 (IASI apodized noise divided by 2)

Table 8: S4 (GEO) TIR instrument characterization.

IASI-NG (called in the paper S5-TIR): the spatial sampling for IASI-NG (called in your paper S5-TIR) is not correct. The spatial sampling for IASI-NG is the following (the same as for IASI): circular pixels of 12 km of diameters whose centers are spaced by 25 km at nadir. Figure 1 of the paper shows 5 pixels within 0.5 ° of latitude and that is not possible. One may have at best 3 pixels and typically 2 pixels within 0.5 ° (which is roughly 55 km) in both directions (along and across the satellite track). Therefore, it is not possible to have so many IASI-NG pixels within a box of 0.5° x 0.625°, but half of them. Therefore, the number of measurements used for the fusion for the given box is not correct. The spacing of the IASI-NG pixels must be corrected and the results should be revised.

S5-TIR products are simulated according to [D4], [D42] and [D6] and their characteristics are summarized in [D3.4] from which we extracted the following table 4.

	LEO (S5)	GEO (S4)
Field of view (km^2) G/T	5×5 / 12×12	5×5 / 15×15

Table 4: *Instrument characterization for LEO and GEO TIR measurements. Goal (G) and Threshold (T) values indicated in the table correspond, respectively, to estimates of the parameters in case the instrument performs at its best and to limit values that we expect to reach anyhow. AURORA will be using Threshold values for generation of simulated data.*

We assumed that the pixel had a square shape with a side of 12 km at nadir (and no spacing between them) and with that configuration, you can have about five pixels in latitude direction in a 0.5-degree grid box. The same general considerations of the previous two points apply here.

UVNS (called in the paper S5-UV): The horizontal sampling of UVNS pixels is not correct either. As announced by ESA https://earth.esa.int/web/eoportal/satellite-missions/c-missions/copernicus-sentinel-5, the horizontal sampling of UVNS is 7 km x 7 km which is much smaller than the box of 0.5 x 0.625° in Fig. 1. Therefore, it is not possible that no pixel is available for UVNS (as indicated in the current version of the manuscript).

S5-UV products are simulated according to [D4], [D42] and [D6] and their characteristics are summarized in [D2.1] from which we extracted the following table 3.2.4. Regarding the reviewer comment on 7x7 km pixel size: this refers to S5-UV2 (300-320 nm) band while S5-UV1 band (270 - 300nm) has pixel of about 50x50 km. Within AURORA, we took S5-UV1 band as reference target, and with a pixel size of 45x45 km it is possible not to have a pixel centre in a 0.5-degree grid box.

	LEO (S5)	GEO (S4)
Spectral range (nm)	270-320	305-320
spectral resolution (nm)	LEO-UV1: 1.0 (270-300nm) LEO-UV2: 0.5 (300-320nm)	0.5
Spectral sampling ratio	3	3
SNR radiance	LEO-UV1: 100 @ 270 nm LEO-UV2: 1000 @ 310 (G) / 320 (T) nm	305 nm: 200 (G) / 160 (T) 310 nm: 400 (G) / 320 (T) 315 nm: 700 (G) / 630 (T) 320 nm: 900
SNR irradiance	10000	305 nm: 3000 (G) / 1000 (T) 310 nm: 3000 (G) / 1600 (T) 315 nm: 10000 (G) / 2000 (T) 320 nm: 10000 (G) / 2700 (T)
Spatial sampling distance	LEO-UV1: 50 (T) / 15 (G) km LEO-UV2: 15 (T) / 7 (B) / 5 (G) km	<= 8 km at 45°N and longitude of the satellite (0°E)
Geographical coverage	Continuous measurement on the illuminated side of the Earth's atmosphere, OZA <= 66°, performance requirements valid for SZA < 80°.	Longitude: 30°W – 40°E @ 40N Latitude: 25°N (G) / 30°N (T) – 65°N @ 0°E Rectangular in view angles, areas with OZA > 75° not required We ignore here any southward/northward shifts in winter/summer

.

Table 3.2.4: Instrument characterization for LEO and GEO UV measurements. Goal (G) and Threshold (T) values indicated in the table correspond, respectively, to estimates of the parameters in case the instrument performs at its best and to limit values that we expect to reach anyhow. AURORA will be using Threshold values for generation of simulated data.

For avoiding all these errors, I strongly recommend using the real names of the instruments: UVNS/Sentinel 5, UVN/Sentinel 4, IASI-NG/EPS-SG and IRS/MTG-S, or at least part of their real names. In my opinion, creating new names that are only used in this paper only add confusion. In addition, "Sentinel" only refers to the UV-VIS instruments and not the TIR. Of course, the spectral resolution and horizontal sampling for each of them must be corrected.

Since now it should be clear that we are referring to instruments whose characteristics are not aligned with the most recent specifications, we think it is appropriate to keep the terminology unchanged also to avoid generating further misunderstandings. To further help the reader, we added a new table (Table 1) that reports the more relevant instrumental parameters (cited in the previous answers) together with the adopted terminology.

Another major point concerns the explanation of the results of Figure 3 of the manuscript. In the revision, a new paragraph explains the gain of sensitivity in the Fused product with respect to the L2 retrievals. However, they do not explain two key points: At the lowest point (1000 hPa) and near the highest (0.5 hPa) the AK for the fused product is much stronger than the ones of the L2 products. At 1000 hPa, a local minimum is seen for the AK of all the L2 products

(S4-TIR, S5-TIR and S4-UV), however the AK shows a relative maximum more than twice larger than the best case of the L2 products. At 0.5 hPa, the AK of the Fused product is 5 or 6 times larger than the individual L2 products. Elsewhere, the AK enhances by about 30 or 50 %, but not by a factor 2 or 6. Could you explain in the detail these features? Is this only a numerical feature of this single profile? What are the physical reasons for such an extremely large enhancement of sensitivity? and where would the information come from? Moreover, why vertical resolution in Fig. 3 right panel (FUS product) is the finest at 1000 hPa (above it is coarser)? This is never the case for any L2 product of ozone derived by optimal estimation or Tikhonov-Philips regularization. I cannot understand such a performance of the Fusion algorithm, which is not consistent with those of the original products. This should be clearly and thoroughly demonstrated.

In the past revision, we added a new figure (Figure 4) to explain the enhancements obtained with the CDF in terms of vertical resolution, and even if this figure refers to different vertical levels (400 and 4 hPa) with respect to the ones that the referee mentions (1000 and 0.5 hPa) it represents the same effects noted by the reviewer.

In the paper, we recognized three distinct phenomena to which the DOFs increase can be attributed. The first is the constriction of the main FUS AK lobe and the consequent improvement of the vertical resolution with respect to L2 products. The second phenomenon relates to the fact that while for the FUS product the maximum value of the AK row corresponds to its diagonal element, for the L2 products these maxima are shifted with respect to the reference altitude of the rows. The last phenomenon is a stronger contribution of the measurements with respect to the a priori in the FUS product.

Here we repeat the same figure for the two vertical levels of interest. As in figure 4, at lower altitudes (1000 hPa, left panel) the three phenomena coexist: while for the FUS product the maximum value of the AK row corresponds to its diagonal element, the L2 maxima are shifted with respect to the reference altitude of the rows; also note that the peak of the FUS row tends to be narrower than the L2 ones resulting in a better vertical resolution. This is also the reason why the vertical resolution of the FUS product has its finest value at 1000 hPa, and this not happens to the L2 products. Considering the sum of all the value of the considered AK row we have 1.06 for the FUS and 0.82 for the L2.

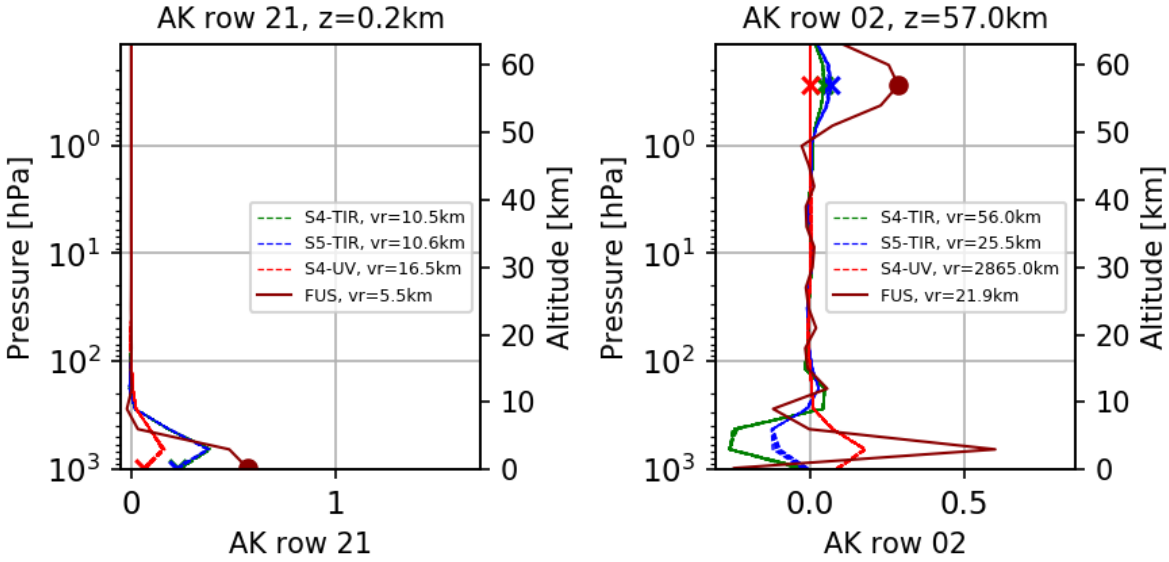

At higher altitudes (0.3 hPa, right panel) the results also depend on the shape of the AK rows that exhibit large secondary lobes; here the main reason of the DOFs increase seems to be a stronger contribution of the measurements with respect of the a-priori. The large secondary lobes located at lower altitudes affect the values of the sum of the AK row (1.20 for FUS and vs 0.37for L2).

These results depend mainly on the particular shape of the L2 AK rows so can be considered a numerical feature of this particular situation; on the other hand, the left panel of figure 7 (in the paper) and S7 (in the supplementary material) clearly show that they primarily depend on the FUS type and on the number of L2 fusing products. In these figures it is also evident that SF AK values larger than 10 are relatively common in the results relative to the considered dataset.

Title: it is written "the Copernicus Atmospheric Sentinel missions" but it is not precise. The paper only refers to EPS-SG and MTG-S missions. There are other Sentinel missions that are used for the atmosphere which are not analyzed in the paper: Sentinel 5 Precusor/TROPOMI, Sentinel 3 SLSTR and there will probably be other atmospheric sentinel missions in the future. Therefore, the title should be revised: "the Copernicus Atmospheric Sentinel missions" should be replaced by EPS-SG and MTG-S missions.

We propose the following new title: "APPLICATION OF THE COMPLETE DATA FUSION TO THE OZONE PROFILES MEASURED BY GEOSTATIONARY AND LOW EARTH ORBITS SATELLITES: A FEASIBILITY STUDY"

Section 3.2: Please correct "contribute of the measures" … by "contribution of measurements"

done

Keep the same nomenclature for averaging kernels: AK or AKM, but do not use both.

AKM removed

Although requested in the previous review, authors provided only scarce additional information on "Atmospheric scenario" in section 2.1. A more detailed description of the used models should be provided.

In the paper we provided the reference in which the atmospheric scenario is described and the reader, if interested, can deepen there the details of the used models. Moreover, we described the role of the scenario both in the L2 product simulation and in the CDF, also explicating the role of the virtual truth in the equations. On the other hand, we prefer not to report a more detailed description in the paper because not relevant to the main focus of the paper.

This sentence and others are not correct "… ozone profiles measured in the UV region" Ozone is not measured in a spectral region. Please replace by "ozone profiles derived from measurements in the UV region"

done.

In the reply, please cite every change in the response to the reviewer's documents and the lines where they are. Otherwise, it is very difficult to track the changes done.

Done (see also the list below).

Last sentence of abstract may be cut into two.

done.

Relevant change list

- Title change
- Added a paragraph at the end of **1 Introduction** to introduce the fact that the simulated L2 products are not exactly aligned with the actual specifications (lines 80-86).
- Added a new paragraph **2.3 L2 Product Technical Specifications**, regarding the technical specification on which the L2 product simulation is based, also to better explain the fact that the simulated L2 products are not exactly aligned with the actually foreseen specifications. Lines 140-159
- Added a table (Table 1) in **2.3 L2 Product Technical Specifications** to summarize the instrument parameters that are more relevant for the L2 simulation.
- Added three new references in paragraph 2.3: (ESA 2012a, ESA 2012b, EUMETSAT 2010), lines 146, 423-430.
- Added a paragraph at half **2.3 The CDF method** to explain the choice of $\mathbf{S_{coinc}}$ (lines 176-180).

Application of the Complete Data Fusion to the ozone profiles measured by geostationary and low earth orbits satellites: a feasibility study~~Application of the Complete Data Fusion to the ozone profiles measured by the Copernicus Atmospheric Sentinel missions: a feasibility study~~

Nicola Zoppetti[1], Simone Ceccherini[1], Bruno Carli[1], Samuele Del Bianco[1], Marco Gai[1], Cecilia Tirelli[1], Flavio Barbara[1], Rossana Dragani[2], Antti Arola[3], Jukka Kujanpää[4], Jacob C.A. van Peet[5,6], Ronald van der A[5] and Ugo Cortesi[1]

[1] Istituto di Fisica Applicata "Nello Carrara" del Consiglio Nazionale delle Ricerche, Via Madonna del Piano 10, 50019 Sesto Fiorentino, Italy
[2] European Centre for Medium-Range Weather Forecasts, Shinfield Park, Reading, RG2 9AX, UK
[3] Finnish Meteorological Institute, Atmospheric Research Centre of Eastern Finland, P.O.Box 1627, 70211 Kuopio, Finland
[4] Finnish Meteorological Institute, Space and Earth Observation Centre, P.O. Box 503, FI-00101 Helsinki, Finland
[5] Royal Netherlands Meteorological Institute, Utrechtseweg 297, 3731 GA De Bilt, The Netherlands
[6] Vrije Universiteit Amsterdam, Department of Earth Sciences, Amsterdam, The Netherlands

Correspondence to: Nicola Zoppetti (N.Zoppetti@ifac.cnr.it)

Abstract. The new platforms for Earth observation from space are characterized by measurements made with great spatial and temporal resolution. While this abundance of information makes it possible to detect and study localized phenomena, on the other hand, it may be difficult to manage this large amount of data in the study of global and large-scale phenomena.

A particularly significant example is the use by assimilation systems of Level 2 products that represent gas profiles in the atmosphere. The models on which assimilation systems are based are discretized on spatial grids with horizontal dimensions of the order of tens of kilometres in which tens or hundreds of measurements may fall in the ~~near~~ future.

A simple procedure to overcome this problem is to extract a subset of the original measurements but this involves a loss of information; another option is the use of simple averages of the profiles, but also this approach has some limitations that we will ~~be~~ discuss~~ed~~ in the paper. A more ~~refined~~ advanced solution is to resort to the so-called fusion algorithms, capable of compressing the size of the dataset while limiting the information loss. A novel data fusion method, the Complete Data Fusion, was recently developed to merge a ~~-~~posteriori a set of retrieved products in a single product. In the present paper, we apply the Complete Data Fusion method ~~is applied~~ to ozone profile measurements simulated in the thermal infrared and ultraviolet bands, in a realistic scenario, according to the specifications of the Sentinel 4 and 5 missions of the Copernicus programme. Then the fused products are compared with the input profiles; comparisons show that the output products of data fusion have in general smaller total errors and higher information contents. The comparisons of the fused with the fusing products are presented both at single fusion grid-box scale and with a statistical analysis of the results obtained on large sets of fusion grid-box of the same size. ~~and~~ ~~t~~We also evaluate the grid box size impact ~~was also evaluated~~, showing that the Complete Data Fusion method can be used with different grid-box sizes even if this possibility is ~~strictly~~ connected to the natural variability of the considered atmospheric molecule.

1. Introduction

In the context of the Copernicus programme (https://www.copernicus.eu) ~~of~~ coordinated by the European Commission, the European Space Agency is responsible for the Space Component consisting of a novel set of Earth Observation (EO) satellite missions for environmental monitoring applications: the Sentinels (https://sentinel.esa.int/web/sentinel/missions). Each mission focuses on a specific aspect of EO. In particular, the geostationary mission Sentinel-4 (S4) and the two Low Earth

Orbit missions (Sentinel-5p and Sentinel 5 (S5)), referred to as the atmospheric Sentinels, are dedicated to monitoring air quality, stratospheric ozone, ultraviolet surface radiation and climate.

The atmospheric Sentinels will provide an enormous amount of data with unprecedented accuracy and spatio-temporal resolution. In this scenario, a central challenge is to enable a generic data user (for example, an assimilation system) to exploit such a large amount of data.

A variety of approaches can serve the purpose to convey in a single product the information associated withto remote sensing observations of the vertical distribution of a given atmospheric target from multiple independent sources. Despite the fact that methodologies to combine coincident measurements from vertical sounders developed to a relatively lesser extent compared to similar classes of algorithms applicable to imaging systems, they are of great and increasing importance to respond to the need for full exploitation of data from new satellites, such as the Copernicus Sentinels and contributing missions. Strategies forfor the combined use of multiple atmospheric profile datasets encompass frominclude a posteriori data fusion techniques to synergistictechniques, synergistic inversion processes (Aires et al., 2012 and references therein; Natraj et al., 2011; Cuesta et al., 2013; Cortesi et al., 2016; Sato et al., 2018), and, in broader terms, might include assimilation systems with their unique capability of gap filling by merging model and experimental data (Lahoz and Schneider, 2014).

These three different approaches differ in the accepted inputs and in the involved models. In the synergistic inversion, the inputs consist in of the radiance observations (Level 1 products) of all the involved measurements and the output profiles are obtained by a simultaneous retrieval of these observations. A A posteriori fusion techniques consist in of sophisticated averaging processes in which the inputs are profiles (Level 2 products) retrieved from the single measurements. The assimilation techniques, in their more general implementations, can accept as inputs both radiances and profiles and use the information of the measurements as inputs of an atmospheric model. Each of these strategies clearly implies different advantages and drawbacks, ultimately assessing the cost-to-benefit ratio that drives the selection of the option of choice for the specific case under investigation.

In particular Data fusion algorithms, such as the Complete Data Fusion (CDF) (Ceccherini et al., 2015), can be particularly well suited to reduce the data volume that users need to access and handle while retaining the information content of the whole level 2 (L2) products.

The CDF inputs is are any number of L2 profiles retrieved with the optimal estimation technique and characterized by their a -priori information, covariance matrix (CM) and averaging kernel (AK) matrix. The output of the CDF is a single product (also characterized by an a- priori, a CM and AK matrices) in which collects all the available information the vertical sensitivity increases and the error reduces with respect to the inputs (Ceccherini et al., 2015). content.

This work is based on the simulated data produced in the context of the Advanced Ultraviolet Radiation and Ozone Retrieval for Applications project (AURORA, Cortesi et al.,2018), funded by the European Commission in the framework of the Horizon 2020 programme. The project regards the sequential application of fusion and assimilation algorithms to ozone profiles simulated according to the specifications of the atmospheric Sentinels.

The use of synthetic data allows evaluating the performances of the algorithms also in terms of differences between the products of interest and a reference truth, represented by the atmospheric scenario used in the L2 simulation procedure to simulate the L2 products. On the other hand, the absence of systematic errors in the simulated measurements limits the study to ideal measurement conditions. However, the CDF algorithm intrinsically provides a mechanism to include different kinds of errors into the analysis. For instance, Ceccherini et al. (2018) discussed how to treat interpolation and coincidence errors can be accounted for , whileand Ceccherini et al. (2019) explicitly introduces the treatment of systematic errors.

This work is divided into two parts. In the first part, we describe the datasets and methodologies (the L2 simulation procedure and the CDF) used in the present paper and discuss the differences between CDF and mere averagingand discuss the use of the profiles average as fusion technique. In the second part, the quality of the fused products obtained from L2 profiles that are not perfectly co-located in space and in time is analyzsed. To account for the geo-temporal differences in the L2 profiles,

a coincidence error is added to the fused product error budget. The fused and standard L2 products are compared and assessed in terms of their information content, highlighting the better data quality provided by the fusion. Finally, we also show that the CDF can be applied with different coincidence grid-box sizes, allowing for different compression factors of the Level 2 input data volume.

It is important to note that the specifications used to simulate L2 products were the state of the art at the time of their usage in the AURORA project context, but are now out of date. It follows that some of the characteristics of the products used in this work differ from what they will be in reality. Nevertheless, this work focuses on a comparison of the fused and L2 products and, in particular, on the ability of the CDF inducing quality improvements that are, in some sense, independent from precise instrumental characteristics.

The application of CDF to L2 products simulated with the characteristics even only similar to the one expected from the atmospheric Sentinel 4 and 5 allows establishing the possible benefits in case of real Sentinel data.~~The application of CDF to L2 products simulated with the characteristics expected from the atmospheric Sentinel 4 and 5 allows to establish the possible benefits in case of real Sentinel data.~~

2. Material and methods

2.1. Atmospheric scenario and ozone climatology

In this work, we used t~~T~~wo basic external sources ~~have been used~~ to generate the database of the standard L2 ozone products~~: used in this work :~~ the ozone climatology and the atmospheric scenario.

We used t~~T~~he ozone climatology ~~was used~~ as a priori information ~~for~~ in both the simulation of L2 products and ~~the calculation of~~ the CDF. The atmospheric scenario represents the true state of the atmosphere, and ~~is used~~we used it ~~for~~ in both the simulation of L2 products and the quality assessment of the fused ones.

~~The~~ In particular, the ozone climatology was derived from McPeters and Labow (McPeters and Labow, 2012) and directly ~~provides~~ provided the a priori profile x_a used either in the simulation expressions (Eq. (1)), as well as in the fusion (see Eq. (6)). We calculate the diagonal terms of the a priori CM~~The CM of the a priori profile~~ $\mathbf{S}_a$ ~~is obtained setting the diagonal terms equal to~~as the square of the standard deviation of McPeters and Labow climatology~~-~~, putting an inferior limit to this diagonal value equal to the square of 20% of the a priori profile.~~where this standard deviation is larger than 20% of the a priori profile and to the square of 20% of the a priori profile otherwise.~~ The off-diagonal elements are calculated using a correlation length of 6 km. The correlation length is used to reduce oscillations in the simulated profiles, and ~~the value of~~ 6 km is the typical value~~ly~~ used for nadir ozone profile retrieval (Liu et al., 2010, Miles et al., 2015). The a priori CM is used in the ~~simulation of the L2 products, and in particular~~ in the expression of the L2 AK matrix (Eq. (2)) and in ~~the CMs of~~ Eq. (4) and (5) of the next paragraph. The a priori CM $\mathbf{S}_a$ plays an important role also in the CDF equations (see Eq. (6)).

The atmospheric scenario is taken from the Modern Era-Retrospective analysis for Research and Applications version 2 (MERRA2) reanalysis (Gelaro et al., 2017). The MERRA2 data are provided by the Global Modelling and Assimilation Office (GMAO) at NASA Goddard Space Flight Center. This reanalysis covers the recent time of remotely sensed data, from 1979 through the present. The atmospheric scenario is the source of true profile $\boldsymbol{x}_t$ used in Eq. (1) to ~~synthetize~~ synthesize the simulated L2 products and represents the main reference for the comparison of the quality of L2 and fused products.

2.2. L2 Product Simulation Algorithm

The simulation algorithm has been originally formalized in the context of the AURORA project, aiming at an efficient computational process. The L2 retrieved state is simulated on a fixed vertical grid with a 3 km step, by the linear approximation given in Eq. (1):

$$\hat{\boldsymbol{x}} = \mathbf{A}\boldsymbol{x}_t + (\mathbf{I} - \mathbf{A})\boldsymbol{x}_a + \boldsymbol{\delta} \quad (1)$$

In Eq. (1), ~~where~~ $\boldsymbol{x}_t$ is the true state of the atmosphere represented by the atmospheric scenarios, $\boldsymbol{x}_a$ is the a priori estimate of the state vector provided by the ozone climatology, $\boldsymbol{\delta}$ is the uncertainty in the retrieved value due to measurement noise, and $\mathbf{A} = \partial\hat{\boldsymbol{x}}/\partial\boldsymbol{x}_t$ is the AK matrix (Rodgers, 2000) calculated according to Eq. (2)~~:~~.

$$\mathbf{A} = \left(\mathbf{K}^T\mathbf{S}_y^{-1}\mathbf{K} + \mathbf{S}_a^{-1}\right)^{-1}\mathbf{K}^T\mathbf{S}_y^{-1}\mathbf{K} \quad (2)$$

In Eq. (2), **K** is the Jacobian matrix of the forward model, the superscript T represents the transpose operator, $\mathbf{S}_y$ is the CM of the observations and $\mathbf{S}_a$ is the CM of the a priori profile. The retrieval error $\boldsymbol{\delta}$ is calculated applying the gain matrix **G** (Rodgers, 2000) to an error $\boldsymbol{\varepsilon}$ on the observations randomly taken from a Gaussian distribution with average equal to zero and CM given by $\mathbf{S}_y$:

$$\boldsymbol{\delta} = \mathbf{G}\boldsymbol{\varepsilon} = \left(\mathbf{K}^T\mathbf{S}_y^{-1}\mathbf{K} + \mathbf{S}_a^{-1}\right)^{-1}\mathbf{K}^T\mathbf{S}_y^{-1}\boldsymbol{\varepsilon} \quad (3)$$

The CM **S** associated with~~to~~ the retrieval error $\boldsymbol{\delta}$ (introduced in Eq. (3)) is given by Eq. (4) (Rodgers, 2000)~~)~~:

$$\mathbf{S} = \langle\boldsymbol{\delta}\boldsymbol{\delta}^T\rangle = \left(\mathbf{K}^T\mathbf{S}_y^{-1}\mathbf{K} + \mathbf{S}_a^{-1}\right)^{-1}\mathbf{K}^T\mathbf{S}_y^{-1}\mathbf{K}\left(\mathbf{K}^T\mathbf{S}_y^{-1}\mathbf{K} + \mathbf{S}_a^{-1}\right)^{-1} \quad (4)$$

The CM $\mathbf{S}_{total}$ associated with~~to~~ the total error $\boldsymbol{\delta}_{total}$ (that is the difference between the simulated and the true profiles, equal to the random $\boldsymbol{\delta}$ plus the so-called smoothing error, caused by the limited vertical resolution of the measurement; see Eq. (7)), is given by Eq. (5) (Rodgers, 2000):

$$\mathbf{S}_{total} = \langle\boldsymbol{\delta}_{total}\boldsymbol{\delta}_{total}^T\rangle = \left(\mathbf{K}^T\mathbf{S}_y^{-1}\mathbf{K} + \mathbf{S}_a^{-1}\right)^{-1} \quad (5)$$

It should be noted that through the term $\boldsymbol{\delta}$, it is possible to simulate additional error components with respect to the random one considered in this study, and this fact adds flexibility to the simulation method.

In this study, we use the above formulation ~~was used~~ to simulate ozone profiles in ~~the~~ two spectral bands (UV1 and TIR) for both S4 and S5, after considering the instrument specifications and accounting for the differences in the two spectral bands. In particular, ~~if~~ considering a fixed geo-location, ~~is considered, starting from the same~~ true profile and ~~the same~~ a priori information, we obtain the L2 products of the different instruments ~~are obtained~~ by ~~the~~ choice of ~~of the suitable Jacobian matrix~~ **K** and ~~of the CM~~ $\mathbf{S}_y$, that have been synthetized using the technical requirements of the considered platforms and their foreseen performances.

2.3. L2 Product Technical Specifications

~~It is important to remind here that~~In the context of Sentinel missions, the ozone profiles derived from measurements~~d~~ in the UV region will be retrieved from spectral radiances acquired by the UVNS/Sentinel-5 spectrometer on-board Meteorological Operational satellite - Second Generation (MetOp-SG) and by the UVN/Sentinel-4 spectrometer on-board Meteosat Third Generation Sounder (MTG-S). For ozone and other targets observed in the TIR, the atmospheric Sentinel missions will ~~be using~~use the operational products of IASI-NG on MetOp-SG and of IRS on MTG.

~~In the framework of the AURORA project, simulated ozone products from the above-mentioned instruments operating in the UV and TIR regions were generated by using the most up-to-date information available.~~ In the framework of the AURORA

project, we simulated ozone products from the instruments mentioned above, by using the information available at the beginning of 2016 (ESA 2012a, ESA 2012b, EUMETSAT 2010, Crevoisier et al. 2014). These specifications are now partially outdated and, besides, we applied to them some simplifications: for example, we considered only UV1 band (neglecting UV2, 300-320 nm) and the shape of the pixels is supposed to be a square at nadir. Consequently, the dataset of simulated L2 products is not exactly in line with the specifications currently foreseen for the instruments of interest. Table 1 reports some of the more relevant characteristics of the simulated measurements. It is worth to note that when an instrumental parameter has both a Goal value (the value in case the instrument performs at its best) and a Threshold value (the value that we expect to reach anyhow), the latter is used for the simulation.

A more detailed description of the instrumental and observational features~~, as well as of the characteristics of different L2 products~~ goes beyond the scope of this article. All the relevant information was reported in the Technical Note on L2 Data Simulations (AURORA 2017) and can also be found in (Cortesi et al., 2018). ~~and in table 1 of (Tirelli et al 2020), where the spectral bands and the available products specifications used in for the simulation of ozone products in the context of the AURORA project are summarized.~~

~~For the sake of shortness, i~~In table 1 and in the next sections of the paper, we ~~will~~ refer to UVNS/MetOp-SG as S5-UV1, to UVN/MTG as S4-UV1, to IASI-NG/MetOp-SG as S5-TIR and to IR/MTG as S4-TIR. Since we simulated instruments with characteristics that differ from their most recent specifications, we think it is appropriate to use an independent terminology also to avoid misunderstandings.

~~2.3.~~2.4. The CDF method

In this s~~S~~ection, we briefly recall the formulas of the CDF method (Ceccherini et al., 2015). We assume to have N independent simultaneous measurements of the vertical profile of an atmospheric species that ~~can be referred~~refer to the same geo-location. Performing the retrieval of the N measurements, we obtain N vectors $\hat{\boldsymbol{x}}_i$ (i=1, 2, …, N) providing independent estimates of the profile, here assumed to be represented on a common vertical grid. Using as inputs these N measurements, the CDF produces as output a single product characterized by a profile $\boldsymbol{x}_f$, an AK matrix $\mathbf{A}_f$ and a CM matrix $\mathbf{S}_f$ with the procedure summarized by Eq~~.~~s. (6). These three quantities are ~~function of~~dependent on the input products, $\mathbf{A}_i$, $\mathbf{S}_i$, hereafter referred to as fusing products, and depend on the a priori information ($\boldsymbol{x}_a$, $\mathbf{S}_a$) used as a constraint for the fused product.

$\boldsymbol{\alpha}_i = \hat{\boldsymbol{x}}_i - (\mathbf{I} - \mathbf{A}_i)\boldsymbol{x}_{ai} = \mathbf{A}_i\boldsymbol{x}_t + \boldsymbol{\delta}_i + \mathbf{A}_i\boldsymbol{\delta}_{coinc,i}$	(6a)
$\tilde{\boldsymbol{S}}_i = \mathbf{S}_i + \mathbf{A}_i\mathbf{S}_{coinc,i}\mathbf{A}_i^T$	(6b)
$\boldsymbol{x}_f = \left(\sum_{i=1}^{N}\mathbf{A}_i^T\tilde{\mathbf{S}}_i^{-1}\mathbf{A}_i + \mathbf{S}_a^{-1}\right)^{-1}\left(\sum_{i=1}^{N}\mathbf{A}_i^T\tilde{\mathbf{S}}_i^{-1}\boldsymbol{\alpha}_i + \mathbf{S}_a^{-1}\boldsymbol{x}_a\right)$	(6c)
$\mathbf{A}_f = \left(\sum_{i=1}^{N}\mathbf{A}_i^T\tilde{\mathbf{S}}_i^{-1}\mathbf{A}_i + \mathbf{S}_a^{-1}\right)^{-1}\sum_{i=1}^{N}\mathbf{A}_i^T\tilde{\mathbf{S}}_i^{-1}\mathbf{A}_i$	(6d)
$\mathbf{S}_f = \left(\sum_{i=1}^{N}\mathbf{A}_i^T\tilde{\mathbf{S}}_i^{-1}\mathbf{A}_i + \boldsymbol{S_a^{-1}}\right)^{-1}\sum_{i=1}^{N}\mathbf{A}_i^T\tilde{\mathbf{S}}_i^{-1}\mathbf{A}_i\left(\sum_{i=1}^{N}\mathbf{A}_i^T\tilde{\mathbf{S}}_i^{-1}\mathbf{A}_i + \mathbf{S}_a^{-1}\right)^{-1}$	(6e)

$$\mathbf{S}_{f\,total} = \left(\sum_{i=1}^{N} \mathbf{A}_i^T \tilde{\mathbf{S}}_i^{-1} \mathbf{A}_i + \boldsymbol{S}_a^{-1} \right)^{-1} \quad (6f)$$

~~For what concern~~Concerning the profile and the error, we can consider the CDF ~~can be thought~~ as a "smart average" in which the a priori information is removed from the L2 profiles and CMs before they are put together in the average. The total error of the L2 product without a priori is higher than the original one, and the effect of the average only partially compensates this error increase. ~~The total error of the single product whose a priori information has been removed is higher than the original one and this error increase is only partially compensated by the effect of the average.~~ Consequently~~This is the reason why~~, even if the total error of the fused product is generally lower than the one of the single L2 fusing product, it is in general higher than the error of the average. The behaviour of the AK matrix is less intuitive, and we will thoroughly analyse it ~~and will be thoroughly analysed~~ in the presentation of the results.

If the input products are not coincident in time and space, the CDF introduces a~~A~~ coincidence error characterized by a CM $\mathbf{S}_{coinc}$ ~~is added if the input products are not coincident in time and space~~. ~~When the CDF is applied to not perfectly coincident products,~~In this work, we calculated the diagonal elements of $\mathbf{S}_{coinc}$ ~~are calculated~~ as the square of the 5% of the a priori profile $\boldsymbol{x}_a$, where we ~~;~~ choose this value ~~has been chosen~~ considering the size of the coincidence grid cells used in this study. We calculate ~~T~~the off-diagonal elements of $\mathbf{S}_{coinc}$~~,~~ ~~are obtained~~ applying an exponential decay with a correlation length of 6 km (Ceccherini et al. 2018).~~-~~ The 5% choice matured in a heuristic way by varying the percentage value and observing the quality of the fused product in some single reference cells and by looking at the entire dataset in representations similar to figures 6 and 7.

The~~In (Ceccherini et al. 2019) the~~ dynamical choice of $\mathbf{S}_{coinc}$ is presented in (Ceccherini et al. 2019). I~~and i~~n particular the a priori error (coincident with the climatological variability) is used as the reference for the diagonal elements and a fixed exponential decay is applied too. However, ~~but~~ the multiplicative factor is calculated by imposing that the cost function of the retrieval is equal to its ~~expectation~~ expected value. That study, which is based on simulated products similar to the ones of this work, shows that even if the coincidence error is strictly needed for the correct behaviour of the CDF product, this is not strongly dependant by its exact amount until it is smaller than ~~with respect to~~ the errors of the individual L2 products.

The formulas of Eqs. (6) refer to the case of measurements made on the same vertical grid. In general, also an interpolation error may be needed considering that the retrievals of the products to be fused can be ~~furnished~~ defined on different vertical grids. In (Ceccherini et al. 2018) the general expressions of CDF in the case of the fusion of products characterized by different vertical grids are presented and discussed together with the expression of the interpolation error that depends on the involved grids and ~~on~~ the AK matrices of the fusing products. However, since the interpolation error does not apply to the present study (we simulated all the L2 products ~~have been simulated~~ on the same vertical grid), it has not been considered in Eqs. (6) and in the following discussion.

~~2.4.~~2.5. Arithmetical average and biases

Before proceeding, it is necessary to clarify why the arithmetic average of the profiles cannot be considered as a good option to represent a set of products retrieved with optimal estimation techniques.

To do this, we consider N coincident L2 measurements (i=1,..,N) referring to the same true profile, the same AK matrix and the same CM but having different (noise) errors $\boldsymbol{\delta}_i$ randomly generated according to Eq. (3). The total error expression for the *i-th* measurement is given in Eq. (7) that can be easily derived from Eq. (1).

$$\boldsymbol{\delta}_{i,\mathrm{total}} = \hat{\boldsymbol{x}}_i - \boldsymbol{x}_t = (\mathbf{I} - \mathbf{A}_i)(\boldsymbol{x}_a - \boldsymbol{x}_t) + \boldsymbol{\delta}_i \quad (7)$$

Considering that the individual measurements are co-located in space and time, thus they refer to the same truth, the same a priori profile and the same AK matrix **A**, the mean total error is equal to:

$$\langle \boldsymbol{\delta}_{i,\text{total}} \rangle = \langle \hat{\boldsymbol{x}}_i \rangle - \boldsymbol{x}_t = \cdots = (\mathbf{I} - \mathbf{A})(\boldsymbol{x}_a - \boldsymbol{x}_t) + \frac{1}{N}\sum_{i=1}^{N} \boldsymbol{\delta}_i \quad (8)$$

It follows that the averaging process reduces the random component of the total error, but does not reduce the bias due to the a priori information. This bias is equal to the term $(\mathbf{I} - \mathbf{A})(\boldsymbol{x}_a - \boldsymbol{x}_t)$ of Eq. (8), which therefore becomes a dominant component as the number N increases. ~~It follows that the averaging process reduces the random component of the total error, but does not reduce the bias, due to the a priori information and equal to the term $(\mathbf{I} - \mathbf{A})(\boldsymbol{x}_a - \boldsymbol{x}_t)$ of Eq. (8), which therefore becomes a dominant component.~~ The existence of this bias is one of the reasons why the arithmetic ~~mean~~ average cannot be considered as a reference algorithm to collect the information of several products into one. Further reasons concern the choice of a suitable AK matrix to be assigned to the average (see also von Clarmann. and Glatthor 2019) and the management of possible coincidence and interpolation errors. An explicative comparison of the application of CDF and standard averages in the case of 1000 coincident L2 products is reported in the supplementary material.

3. Results and discussion

3.1. Fusion in realistic spatial and temporal resolution conditions: the L2 Datasets

To analyse the behaviour of CDF in realistic spatial and temporal resolution conditions, we consider four sets of measurements ~~were considered~~. These measurements correspond to the ~~cloud~~ cloud-free observations that were possible between 9:00 am and 10:00 am on the 1st April 2012. Table ~~1~~ 2 lists the L2 product types, namely S4-TIR, S4-UV1, S5-TIR and S5-UV1, used in ~~the remaining of th~~this article. The L2 datasets have been generated according to the equations (1)-(5) described in ~~the~~ paragraph 2.2. The details of the simulation process can be explored in the technical note (AURORA 2017) considering that here we simulated all the pixels corresponding to a clear sky line of sight in the atmospheric scenario, without applying any additional selection criteria. In the AURORA project main workstream, we considered four months of data; however, we simulated only a subset of the clear-sky pixels to reduce the computational cost of the simulations (Tirelli et al. 2020). In this AURORA side-study, we consider one hour of data, and we simulate all the clear-sky pixels without additional filters, choosing the orbits so that S4-S5 coincidences occur. The left panel of Figure 5 indirectly represents the spatial distribution of the products simulated for this study. ~~In fact, in the AURORA project 4 months of data have been considered, but a subset of the clear sky pixels has been simulated to reduce the computational cost of the simulations; for this study all the clear sky pixels in the considered hour of data have been simulated, without additional filter, choosing the orbits so that S4-S5 coincidences occur; the spatial distribution of the simulated products is indirectly represented in the left panel of Figure 5.~~

3.2. Single grid-box analysis (0.5ºx0.625º)

We consider ~~first~~ the case of a single grid-box (Figure 1). In the selected grid-box, 118 measurements were available (55 of S4-TIR, 55 of S4-UV1, 8 of S5 TIR, no S5 UV1). The cell has the size of 0.5 degrees in latitude and 0.625 degrees in longitude, centred on the Egina Island in the Aegean Sea. The cell size has been chosen to be comparable with the assimilation grid used in the AURORA project. We assign the geo-location of the fused product to be the barycentre of the horizontal coordinates of the L2 measurements in the grid-box. In this particular case, since the horizontal distribution of the 118 L2 profiles is quite homogeneous, the barycentre is ~~practically~~ placed at the centre of the grid-cell.

Figure 2 shows with green lines the absolute (left panel) and relative (right panel) differences between each L2 profile and the corresponding true profile, with a red line the difference between the fused profile and the mean truth (computed as the average of the 118 true profiles), with a black dash-dotted line the average of the estimated standard deviation of the total error of the individual L2 measurements $\boldsymbol{\sigma}_{total}$, and with a red dash-dotted line the estimated standard deviation of the total error of the fused profile $\boldsymbol{\sigma}_{f\,total}$. The last two quantities have been calculated as the square root of the diagonals of the $\mathbf{S}_{total}$ and $\mathbf{S}_{ftotal}$ CMs given by Eqs. (5) and (6), respectively. Figure 2 shows that the fused product is in better agreement with its truth than the individual profiles with their own, and presents a smaller estimated total error than the individual L2 products. In particular, the right panel allows ~~to see~~seeing in ~~the~~ detail the performances of CDF in the tropospheric region.

The retrieved profile representation is always a compromise between the amplitude of the errors and the vertical resolution.~~The representation of a retrieved profile is always a compromise between the amplitude of the errors and the vertical resolution.~~ The latter can be quantified by the AKs, which ideally would be equal to the identity matrix in the case of a profile that has a vertical resolution equal to that defined by the sampling grid. Diagonal elements with values smaller than 1 correspond to a loss of vertical resolution. In the left panel of Figure 3~~,~~, we compare the diagonal elements of the AKs of the L2 products~~, are compared~~ with the ~~one~~ AK diagonal of the fused product. Here ~~where~~ we have also computed the number of Degrees Of Freedom (DOFs), given by the sum of the diagonal elements of the AK matrix (Rodgers, 2000), for both L2 and fused products, and reported the values in the text box of the left panel.~~; as it can be noted~~Note that the number of DOFs of the fused product is about twice the number of DOFs of the best L2 one. In the right panel of Figure 3,~~,~~ we compare ~~the comparison of~~ the vertical resolution profiles of L2 and FUS products ~~is shown,~~. We calculate ~~where~~ the vertical resolution ~~is calculated~~ starting from AK matrices according to the ~~Full~~ Full-~~Width~~ Width-~~Half~~ Half-Maximum (FWHM) approach (Rodgers, 2000), and in particular with the algorithm defined in (Ridolfi and Sgheri, 2009).

From the comparison of the left and the right panel of Figure 3, it can be noted that the increase of the AK matrix diagonal values of FUS product, and consequently the increase of the number of DOFs, implies an improved vertical resolution only in a subset of the vertical levels. To better understand the effect of the fusion on the AK matrices, it is useful to analyse the behaviour of their ~~individual~~ rows. In Figure 4, two rows are represented, one that refers to the troposphere (left panel, 6 km) one to the middle stratosphere (right panel, 39 km), where the reference altitude is the one corresponding to the diagonal value of the row. The value of the vertical resolution at the considered altitude is reported in the legend (the minimum of vertical resolution at the considered vertical level for each type of L2 product), ~~while~~ and the diagonal value of each row is evidenced in the graphs with cross (L2) and dot markers (FUS). At lower altitudes (left panel), ~~as suggested by one of the reviewers,~~ the DOFs increase can be attributed to three distinct phenomena. The first is the constriction of the main FUS AK lobe and the consequent improvement (of more than 30%) of the vertical resolution with respect to L2 products. The second phenomenon is linked to the fact that~~,~~ while for the FUS product the maximum value of the AK row corresponds to its diagonal element, for the L2 products these maxima are shifted with respect to the reference altitude of the rows. The last phenomenon is a stronger ~~contribute~~ contribution of the (simulated) measurements with respect to the a priori in the FUS product, where the latter effect can be evidenced considering the sum of all the elements of the rows that assume 0.913 as the maximum value for the L2 products and 0.956 for the FUS product. In ~~the~~ this particular case, all these three effects go in such a direction that can be considered as benefits of CDF application. The results at higher altitudes (39 km, right panel) are primarily influenced by the shape of the AK rows that exhibit large secondary lobes that degrade the vertical resolution.

3.3. Statistical analysis for a large domain

While the analysis of the previous paragraph focuses on a particular grid-box, here an analysis of the CDF behaviour is presented, referring to all the 1939 fusion grid-boxes in which more than one of the 79781 L2 simulated products, considered in Table ~~1~~ 2, is placed. The fused products can be classified depending on the types of L2 measurements falling inside the coincidence grid cell. Since S4-TIR and S4-UV1 products are in perfect coincidence and S5-UV1 products have a horizontal

spacing larger than the cell size, only six fused product types (FUS type), listed in Table ~~2~~3, effectively occur. In this table, the FUS type and its description are reported together with the following complementary data:

- Ncells: the number of grid-boxes characterized by the considered FUS type.
- <NL2>: the mean number of individual L2 fusing profiles per grid-box.
- Max NL2: the maximum number of individual L2 fusing products per grid-box.

The left-hand side panel of Figure 5 shows the geographical distribution of the FUS products. Different colours have been used to classify the fused data according to their provenance type. The irregular geographical coverage is due to the realistic distribution of the cloud-~~-~~free measurements. The histogram in the right-hand side panel of Figure 5 shows the number of cells that contain a given number of measurements, divided in different colours depending on the FUS type. The FUS cells, in which only S5 platform L2 products fall, are characterized by a small number of L2 measurements, while when S4 products are present, many L2 measurements can be present.

With the selected grid-box size and the multitude of different products that are present in each cell, the question is which product can be used in alternative to the fusion process in those operations in which a single product is requested in each grid-box. Since the averaging process is affected by a large bias error, a viable alternative is the use of the best fusing product present in the cell, and we want to compare the CDF result with this product. This comparison is the so-called Synergy Factor (SF), introduced by Aires et al. (2012). Although Aires introduces SF only for errors (Eq. (11)), we extend his definition also for other quantities because they constitute a useful tool to synthetically represent the performances of fusion algorithms.

The SF DOF, defined by Eq. (9), is the ratio between the number of DOFs of the FUS product, and the maximum number of DOFs of L2 fusing products. ~~The *SF DOF*, defined by Eq. (9), is a pure number that can be calculated for every FUS pixel by the ratio of the number of DOFs of the FUS product and the maximum number of DOFs of the L2 measurements that have been fused.~~ In this equation, the index l enumerates the vertical levels and the index i enumerates the L2 products fused in each grid-box.

$$SFDOF = \frac{\sum_l \mathbf{A}_{f,ll}}{\max\limits_{i \in L2} \sum_l \mathbf{A}_{ll}} \quad (9)$$

When *SF DOF* is larger than 1.0, the FUS product carries more information than the individual L2 measurements. Figure 6 shows that the *SF DOF* computed for all the fused products (and plotted as a function of the number of L2 profiles in each grid-box) is always larger than 1.0. ~~This means that the information content of the fused product is always larger than that of the standard L2 retrievals.~~ It is also worth noticing that *SF DOF* increases approximately linearly with the logarithm of the number of fusing products, although the proportionality depends on the FUS type. The two different clusters of red symbols (S4:TIR+UV1) are caused by the different latitude bands in which these products are distributed (see also left panel of Figure 5). It is important to underline that the improvement in vertical resolution~~, which cannot be obtained with the arithmetic averaging,~~ is the most demanding requirement ~~(in terms of observation time and instrument sensitivity)~~ in remote sensing observations and, considering the significant gain obtained relative to the single product selection, is the most important feature of fused products.

While *SF DOF* is a scalar quantity, both ***SF AK*** and ***SF ERR***, defined by Eqs. (10) and (11), are vertical profiles of pure numbers. ***SF AK*** represents an expansion on the vertical dimension of *SF DOF* and, in particular, is calculated, level by level, as the ratio between the diagonal elements of the AK matrix of the FUS product and the maximum of the corresponding elements of the AK matrices of the fusing L2 measurements.

A value of ***SF AK*** larger than 1.0 at a specific vertical level (indicated by the index l) means that, at that level, the diagonal value of the AK matrix of the FUS product has a larger value than that of all the individual products. As we have seen

commenting Figure 3 and Figure 4, the increase of the AK diagonal values at a specific level can happen for different reasons, but all of them can be considered as an improvement in the product quality.

$$SFAK_l = \frac{\mathbf{A}_{f,ll}}{\underset{i \in L2}{max}\mathbf{A}_{i,ll}} \quad (10)$$

The ***SF ERR*** (Eq. (11)) at a given level is ~~calculated as~~ the ratio between the minimum total error of the L2 measurements that have been fused and the total error of the FUS product. A value of ***SF ERR*** larger than 1.0 means that, at a specific level, the error of the FUS product is smaller than that of all the individual products.

$$SFERR_l = \frac{\underset{i \in L2}{min}\sigma_{total,i,l}}{\sigma_{ftotal,l}} \quad (11)$$

The SFs defined by Eqs. (10) and (11) provide a conservative comparison because the fused product is compared with the L2 product that at that level has the largest diagonal value in its AK matrix and with the one that has the smallest total error at the same level (generally, these are two distinct L2 products).

Figure 7 shows the ***SF AK*** (left panel) and ***SF ERR*** (right panel) profiles for the 1939 FUS products considered in Table ~~2~~3. We have used different colours to denote the provenance of the L2 data contributing to the fused products and different symbol size to infer the number of L2 fusing measurements (the larger the symbol size, the larger the number of L2 fusing profiles). ~~As mentioned above, the merit of the fused product in terms of SF is higher than that of the L2 retrievals if the ***SF AK*** and ***SF ERR*** are greater than 1.~~ The significant improvement obtained with the fused products is confirmed by Figure 6. In Figure 7, considering symbols of the same colour, the size (N) increases moving horizontally in the graph (same vertical level) from left to right (SF increasing). ~~It can also be noticed that considering symbols of the same colour the symbol size (*N*) tends to increase moving horizontally in the graph (same vertical level) from left to right (SF increasing) denoting~~ This fact denotes that, for each FUS type, SF increases with *N*. This is not in contradiction with the fact that symbols with different colours (FUS types) and different sizes (*N*) can share the same position (SF, vertical level) on the graph. Some ***SF AK*** values, both in the troposphere and in ~~middle~~ the middle-upper atmosphere are smaller than one; in the troposphere, this happens in 20 cells out of 1939 while in the ~~middle~~ middle-upper atmosphere this happens in almost 500 cells for two possible and sometimes simultaneous circumstances. The first one happens when the introduction of the coincidence error provokes a sensible degradation of the quality of the FUS AK matrix~~M~~. The second circumstance happens, for example, when one of the L2 products is characterized by a vertical resolution that is much better than all the other fusing products and, in particular, the peaks of their AK~~M~~ rows tends to not coincide with the nominal vertical level of the row itself.

3.4. Statistical analysis on a coarse horizontal resolution

We have seen that starting from 79781 L2 measurements (Table ~~1~~2), when a coincidence grid-box with size 0.5°x0.625° is used, the number of fused profiles is 1939 (Table ~~2~~3), with a reduction of the data volume of more than a factor 40.

Table ~~3~~ 4 provides a summary of the number of fused profiles and the provenance of the L2 profiles that contribute to them for a fusion grid resolution of 1°x1°. In this case, the total number of FUS products is 775, with a reduction of the data volume of more than a factor 100.

The Synergy factors *SF DOF*, ***SF AK*** and ***SF ERR***, also in this case have been considered, ~~also in this case~~ and the figures (similar to Figure 6 and Figure 7) are reported in the supplementary material. In summary, the greater number of fusing observations in each fusion cell produces a further improvement for both the vertical resolution and the total error. This observation confirms that ~~proving that~~ the CDF method can be used with a wide range of grid-box size and data compression

and the quality of the products generally improves with larger cells. An upper limit to the grid-box size is caused by the coincidence error amplitude, which increases with the geographical variability, degrading the quality of the fused product. T~~;~~ ~~t~~he study of this aspect will be of crucial importance if the CDF will be applied to species with greater spatial-temporal variability than ozone or in any case, to very large spatial-temporal domains.

4. Conclusions

~~T~~This paper presents a feasibility study of the CDF technique applied to L2 products simulated according to the characteristics of the atmospheric Sentinel missions. ~~his paper presents a sensitivity study of the Complete Data Fusion technique, applied to L2 measurements simulated with the characteristics of the measurements, which will be acquired in the context of the atmospheric Sentinel missions.~~ Despite the approximations that characterize the simulated L2 products (technical specifications not exactly in line with the ones of the atmospherics Sentinels and no systematic errors added) this analysis allows to evaluate the performances of the CDF algorithm and to quantify the possible benefits of its application to Sentinel data.~~This analysis allows to evaluate the performances of the CDF algorithm in ideal conditions (i.e., with no systematic errors added) and to quantify the possible benefits of the application of CDF to real Sentinel data.~~

In particular, we show the application of CDF to a single cell with a size of 0.5 degrees in latitude and 0.625 degrees in longitude in which more than 100 L2 products are fused. Results show that the fused product is characterized by higher information content, smaller errors and smaller residuals (i.e., smaller anomalies~~y~~ from the true profiles) compared to individual L2 products. The information content being, with its improvement of the vertical resolution, the most important achievement.

This analysis is then extended to a larger domain consisting ~~in~~ of 79781 L2 products subdivided into 1939 grid boxes with 0.5^{o}x0.625^{o} size. In this case, the comparison of L2 products and CDF output are carried on in terms of synergy factors. This analysis shows that the CDF can be applied to a wide range of situations and that the benefits of the fusion strongly depend on the number of ~~the~~ measurements that are fused ~~together~~ and ~~from~~ on their characteristics. It is also shown that CDF can be run customizing grid resolutions, e.g. to match the resolution requirements of the process that will ingest the products, with full exploitation of all the available measurements.

As the fused products are traced back to a regular, fixed horizontal grid and, as shown here, are not affected by the bias introduced by the a priori information, they can be considered as a new type of Level 3 products with improved quality (reduced bias) and the same characteristics (AK included) with respect to L2 products, even if further analysis ~~are~~ is needed, especially for what concerns the coincidence error to be applied to fus~~e~~ing data on large spatial-temporal domains.

Data availability

The data of the simulations presented in the paper are available from the authors upon request.

MERRA-2 data (atmospheric scenario) are available at MDISC (https://disc.gsfc.nasa.gov)~~-~~, managed by the NASA Goddard Earth Sciences (GES) Data and Information Services Center (DISC).

The ML climatology (McPeters and Labow, 2012) is available online from the Goddard anonymous ftp account: ftp://toms.gsfc.nasa.gov.

Author contributions (according to CRediT https://casrai.org/credit/)

N. Zoppetti: Conceptualization, Methodology, Software, Writing – Original Draft, Writing – Review & Editing, Investigation, Data curation, Visualization S. Ceccherini: Conceptualization, Methodology, Investigation, Writing – Review & Editing B. Carli: Conceptualization, Methodology Writing – Review & Editing, Supervision S. Del Bianco: Investigation, Data curation,

Project Administration M. Gai: Investigation, Data curation C. Tirelli: Investigation, Data curation, Project Administration F. Barbara: Resources R. Dragani: Investigation, Data curation, Writing – Review & Editing A. Arola: Investigation, Data curation J. Kujanpää: Investigation, Data curation R. Van Der A: Investigation, Data curation U. Cortesi: Project Administration, Supervision, Writing – review & editing.

Competing interests.

The authors declare that they have no conflict of interest.

Acknowledgments

The results presented in this paper arise from research activities conducted in the framework of the AURORA project (http://www.aurora-copernicus.eu/) supported by the Horizon 2020 research and innovation programme of the European Union (Call: H2020-EO-2015; Topic: EO-2-2015) under Grant Agreement N. 687428.

Financial support.

This research has been supported by the European Commission, H2020 (AURORA, grant no. 687428).

References

Aires,F., Aznay,O., Prigent,C., Paul,M. and Bernardo,F.: Synergistic multi-wavelength remote sensing versus a posterior combination of retrieved products: Application for the retrieval of atmospheric profiles using MetOp-A. J GEOPHYS RES, Vol. 117, D18304, https://doi.org/10.1029/2011JD017188, 2012.

AURORA consortium, (Advanced Ultraviolet Radiation and Ozone Retrieval For Applications, grant no. 687428): Technical Note On L2 Data Simulations [D3.4], 35 pp., available for download at https://cordis.europa.eu/project/id/687428/results, 2017.

Ceccherini, S., Carli, B., and Raspollini, P.: Equivalence of data fusion and simultaneous retrieval, 2015. Opt. Express, 23, 8476-8488, https://doi.org/10.1364/OE.23.008476, 2015.

Ceccherini, S., Carli, B., Tirelli, C., Zoppetti, N., Del Bianco, S., Cortesi, U., , Kujanpää, J., and Dragani, R.: Importance of interpolation and coincidence errors in data fusion. Atmos. Meas. Tech., 11, 1009–1017, https://doi.org/10.5194/amt-11-1009-2018, 2018.

Ceccherini S., Zoppetti N., Carli B., Cortesi U., Del Bianco S., and Tirelli C.: The cost function of the data fusion process and its application. Atmos. Meas. Tech., 12, 2967–2977, https://doi.org/10.5194/amt-12-2967-2019, 2019.

Cortesi, U., S. Del Bianco, S. Ceccherini, M. Gai, B.M. Dinelli, E. Castelli, H. Oelhaf, W. Woiwode, M. Höpfner, D. Gerber, Synergy between middle infrared and millimeter-wave limb sounding of atmospheric temperature and minor constituents, Atmos. Meas. Tech., 9, 2267-2289, https://doi.org/10.5194/amt-9-2267-2016, 2016.

Cortesi, U., Ceccherini, S., Del Bianco, S., Gai, M., Tirelli, C., Zoppetti, N., Barbara, F., Bonazountas, M., Argyridis, A., Bós, A.,Loenen, E., Arola, A., Kujanpää, J., Lipponen, A., Nyamsi, W.W., van der A, R., van Peet, J., Tuinder, O., Farruggia, V., Masini, A., Simeone, E., Dragani, R., Keppens, A., Lambert, J.-C., van Roozendael, M., Lerot, C., Yu, H., and Verberne, K.: Advanced Ultraviolet Radiation and Ozone Retrieval for Applications (AURORA): A Project Overview, Atmosphere, 9, 454, https://doi.org/10.3390/atmos9110454, 2018.

Crevoisier, C., Clerbaux, C., Guidard, V., Phulpin, T., Armante, R., Barret, B., Camy-Peyret, C., Chaboureau, J.-P., Coheur, P.-F., Crépeau, L., Dufour, G., Labonnote, L., Lavanant, L., Hadji-Lazaro, J., Herbin, H., Jacquinet-Husson, N., Payan, S., Péquignot, E., Pierangelo, C., Sellitto, P., and Stubenrauch, C.: Towards IASI-New Generation (IASI-NG): impact of improved spectral resolution and radiometric noise on the retrieval of thermodynamic, chemistry and climate variables, Atmos. Meas. Tech., 7, 4367–4385, https://doi.org/10.5194/amt-7-4367-2014, 2014.

Cuesta, J., M. Eremenko, X. Liu, G. Dufour, Z. Cai, M. Höpfner, T. von Clarmann, P. Sellitto, G. Foret, B. Gaubert, M. Beekmann, J. Orphal, K. Chance, R. Spurr and J. M. Flaud: Satellite observation of lowermost tropospheric ozone by multispectral synergism of IASI thermal infrared and GOME-2 ultraviolet measurements over Europe, Atmos. Chem. Phys., 13 (19), pp.9675-9693, 2013.

ESA, Mission Science Division, European Space Agency, GMES Sentinels 4 and 5 Mission Requirements Traceability Document (MRTD), EOP-SM/2413/BV-bv, issue 1 rev.0. http://aurora.ifac.cnr.it/utils/personaldocs/see/96/, 2012

ESA, Mission Science Division, GMES Sentinels 4 and 5 Mission Requirements Document (MRD), EOP-SM/2413, issue 1 rev.0. http://aurora.ifac.cnr.it/utils/personaldocs/see/93/, 2012

EUMETSAT, MTG End-User Requirements Document, EUM/MTG/SPE/07/0036, v3C https://www.ncdc.noaa.gov/sites/default/files/attachments/PDF_MTG_EURD.pdf, 2010

Gelaro, R., McCarty, W., Max J. Suárez, M. J., Todling, R., Molod, A., Takacs, L., Randles, C. A., Darmenov, A., Bosilovich, M. G., Reichle, R., Wargan, K., Coy, L., Cullather, R., Draper, C., Akella, S., Buchard, V., Conaty, A., da Silva, A. M., Gu, W., Kim, G. K., Koster, R., Lucchesi, R., Merkova, D., Nielsen, J. E., Partyka, G., Pawson, S., Putman, W., Rienecker, M., Schubert, S. D., Sienkiewicz, M., and Zhao, B. The Modern-Era Retrospective Analysis for Research and Applications, Version 2 (MERRA-2), J. Climate, 30, 5419-5454, https://doi.org/10.1175/JCLI-D-16-0758.1, 2017.

Lahoz, W.A. and Schneider, P., Data assimilation: making sense of Earth Observation, Frontiers in Environmental Science, 2, https://doi.org 10.3389/fenvs.2014.00016, 2014.

Liu, X., Bhartia, P. K., Chance, K., Spurr, R. J. D., and Kurosu, T. P.: Ozone profile retrievals from the Ozone Monitoring Instrument, Atmos. Chem. Phys., 10, 2521-2537, https://doi.org/10.5194/acp-10-2521-2010, 2010.

McPeters, R.D., and Labow, G.J.: Climatology 2011: An MLS and sonde derived ozone climatology for satellite retrieval algorithms, J. Geophys. Res., 117, D10303, https://doi.org/10.1029/2011JD017006, 2012.

Miles, G. M., Siddans, R., Kerridge, B. J., Latter, B. G., and Richards, N. A. D.: Tropospheric ozone and ozone profiles retrieved from GOME-2 and their validation, Atmos. Meas. Tech., 8, 385-398, https://doi.org/10.5194/amt-8-385-2, 2015.

Natraj, V., Liu, X., Kulawik, S., Chance, K., Chatfield, R., Ed-wards, D. P., Eldering, A., Francis, G., Kurosu, T., Pickering, K.,Spurr, R., and Worden, H.: Multi-spectral sensitivity studies for the retrieval of tropospheric and lowermost tropospheric ozone from simulated clear-sky GEO-CAPE measurements, Atmos.Environ., 45, 7151–7165, 2011

Ridolfi,M. and Sgheri,L. 2009: A self-adapting and altitude-dependent regularization method for atmospheric profile retrievals, Atmos. Chem. Phys., 9, 1883–1897, 2009 https://doi.org/10.5194/acp-9-1883-2009

Rodgers, C.D.: Inverse Methods for Atmospheric Sounding: Theory and Practice. Vol. 2 of Series on Atmospheric, Oceanic and Planetary Physics. World Scientific: Singapore, 2000.

Sato, T. O., Sato, T. M., Sagawa, H., Noguchi, K., Saitoh, N., Irie, H., Kita, K., Mahani, M. E., Zettsu, K., Imasu, R., Hayashida, S., and Kasai, Y.: Vertical profile of tropospheric ozone derived from synergetic retrieval using three different wavelength ranges, UV, IR, and microwave: sensitivity study for satellite observation, Atmos. Meas. Tech., 11, 1653–1668, https://doi.org/10.5194/amt-11-1653-2018, 2018.

Tirelli, C., Ceccherini, S.; Zoppetti, N., Del Bianco, S., Gai, M., Barbara, F., Cortesi, U., Kujanpää, J., Huan, Y., Dragani, R. Data fusion analysis of Sentinel-4 and Sentinel-5 simulated ozone data. J. Atmos. Ocean. Technol., 37 (4), 573–587, https://doi.org/10.1175/JTECH-D-19-0063.1, 2020.

von Clarmann, T. and Glatthor, N.: The application of mean averaging kernels to mean trace gas distributions, Atmos. Meas. Tech., 12, 5155–5160, https://doi.org/10.5194/amt-12-5155-2019, 2019.

L2-Type Name	**S4-TIR**	**S4-UV1**	**S5-TIR**	**S5-UV1**
Platform	Meteosat Third Generation Sounder (MTG-S)		Meteorological Operational satellite - Second Generation (MetOp-SG)	
Instrument	Infrared Sounder (IRS)	UV-VIS-NIR Sentinel-4 spectrometer (UVN)	Infrared Atmospheric Sounding Interferometer – New Generation (IASI-NG)	UV-VIS-NIR-SWIR Sentinel-5 spectrometer (UVNS)
Retrieval spectral range	1030-1080 cm^{-1}	305-320 nm	1030-1080 cm^{-1}	270-300 nm
Spectral resolution	0.625 cm^{-1} (apodized IRSF)	0.5 nm	0.25 cm^{-1} (apodized IRSF)	1.0 nm
Spectral sampling ratio	1	3	2	3
Noise Equivalent Brightness Temperature Scenario (according to Crevoisier et al. 2014)	IRS1b		IRS2b	
Signal to Noise Ratio Radiance		160@305 nm (T) 320@310 nm (T) 630@315 nm (T)		100 @270 nm (T,G)

		900@320 nm (T,G)		
Field of View	15×15 km² (T) 5×5 km² (G)	<= 8 km at 45°N and longitude of the satellite (0°E)	12×12 km² (T) 5×5 km² (G)	50x50 km² (T) 15x15 km² (G)
Pixel size used in the simulation (assumed square @ nadir)	8 km		12 km	45 km

Table 1: instrument characterization relevant for the simulation process. Goal (G) and Threshold (T) values correspond, respectively, to estimates of the parameters in case the instrument performs at its best and to limit values that we expect to reach anyhow. AURORA will be using Threshold values for the generation of simulated data.

L2 Type	Number of simulated measurements	Minimal distance between measurements across x along track [km]
S4-TIR	35594	5.7 x 7.4
S4-UV1	35594	
S5-TIR	8023	12.2 x 12.3
S5-UV1	570	46.2 x 46.7
TOTAL	79781	
~~79781~~		

Table 2: ~~Characteristics~~ Number and horizontal resolution of the simulated measurements. For S4 platform across-track is South-North direction, and along-track is East-West direction.

FUS Type	Description	*Ncells*	*<NL2>*	*max NL2*
S4:TIR+UV1	Two or more S4 pixels, no S5 pixels.	908	29.3	160
S4:TIR+UV1_S5:TIR+UV1	Two or more S4 pixels, one or more S5_TIR pixel, one or more S5_UV1 pixel.	245	114.7	163
S4:TIR+UV1_S5:TIR	Two or more S4 pixels, one or more S5_TIR pixel, no S5_UV1 pixels.	299	69.4	165
S4:TIR+UV1_S5:UV1	Two or more S4 pixels, one or more S5_UV1 pixel, no S5_TIR pixels.	2	20	37
S5:TIR+UV1	No S4 pixels, one or more S5_TIR pixels, one or more S5_UV1 pixels.	247	11.1	24
S5:TIR	No S4 pixels, two or more S5_TIR pixels, no S5_UV1 pixels.	238	6.2	14
	TOTAL	1939	41.1	165

Table 3: types and characteristics of the fused product when a coincidence grid cell size of 0.5°x0.625° is used. Ncells is the number of grid-boxes characterized by the considered FUS type; <NL2> is the mean number of individual L2 fusing profiles per grid-box and Max NL2is the maximum number of individual L2 fusing products per grid-box.

FUS Type	Description	N_{cells}	$<NL_2>$	*max NL2*
S4:TIR+UV1	Two or more S4 pixels, no S5 pixels.	354	73.1	420
S4:TIR+UV1_S5:TIR+UV1	Two or more S4 pixels, one or more S5_TIR pixel, one or more S5_UV1 pixel.	140	289.4	504
S4:TIR+UV1_S5:TIR	Two or more S4 pixels, one or more S5_TIR pixel, no S5_UV1 pixels.	79	115.4	442
S4:TIR+UV1_S5:UV1	Two or more S4 pixels, one or more S5_UV1pixel, no S5_TIRpixels.	0	0	0
S5:TIR+UV1	No S4 pixels, one or more S5_TIR pixels, one or more S5_UV1 pixels.	142	26.2	71
S5:TIR	No S4 pixels, two or more S5_TIR pixels, no S5_UV1 pixels.	60	8.9	26

TOTAL	775	102.9	504

Table 4: Like in Table2 but with a grid-box size of 1ºx1º. Ncells is the number of grid-boxes characterized by the considered FUS type; <NL2> is the ~~the~~ mean number of individual L2 fusing profiles per grid-box and Max NL2is the maximum number of individual L2 fusing products per grid-box.

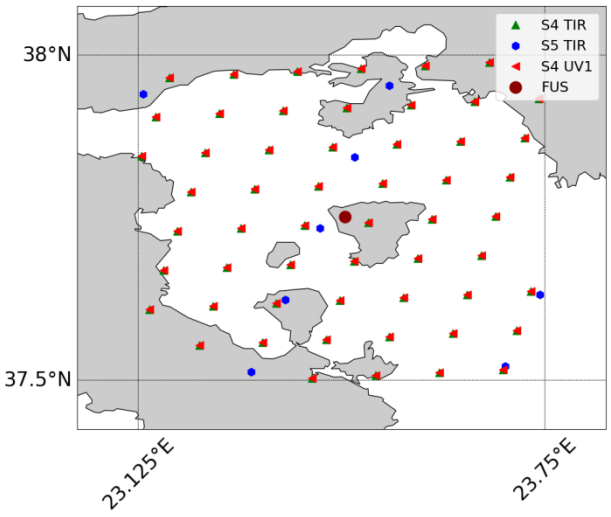

Figure 1: geographical distribution of the simulated L2 measurements and geo-location of the fused product. The black dash-dotted lines represent the borders of the 0.5ºx0.625º grid cells.

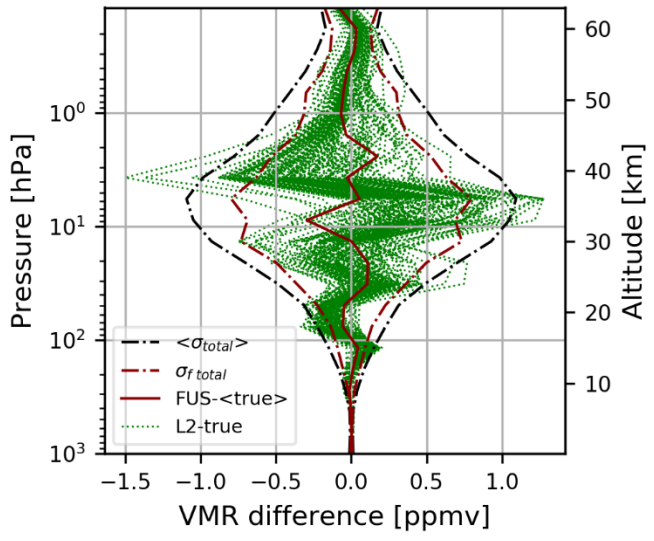

Figure 2 (Left panel): the absolute differences between L2 profiles and their true profiles (green lines), the absolute difference between the fused profile and the average of the true profiles (dark red continuous line), the average of σ_{total} of L2 simulations (black dash-dotted lines), $\sigma_{f\ total}$ (dark red dash-dotted lines). (Right panel): the relative percentage differences between L2 profiles and their true profiles (green lines), the relative percentage difference between the fused profile and the average of the true profiles (dark red continuous line), the average of σ_{total} of L2 simulations normalized wrt the true profile and expressed in percentage (black dash-dotted lines), $\sigma_{f\ total}$ normalized wrt the true profile and expressed in percentage (dark red dash-dotted lines).

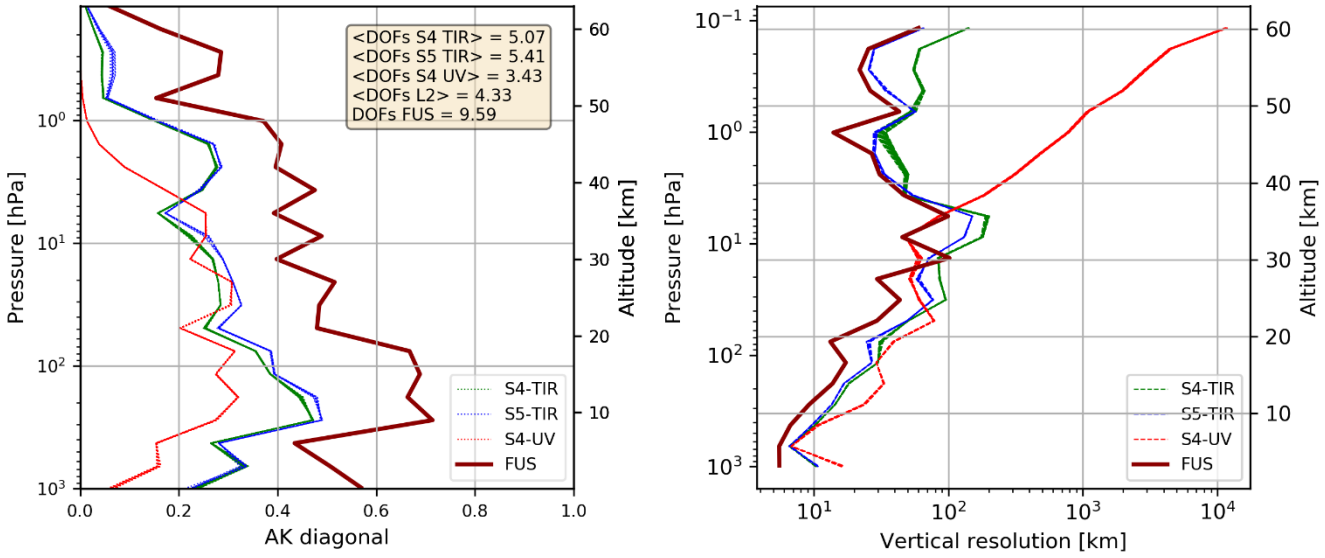

Figure.3 (Left panel): AKs diagonal<u>s</u>. ~~of:~~ S4-TIR products (red lines), S5-TIR products (blue lines) S4-UV products (red lines) and FUS product (dark red line). In the text box<u>,</u> the average number of DOFs for each type of L2 product, the average number of DOFs for all L2 products and the number of DOFs of the FUS product are reported. (Right panel): Vertical resolution (FWHM) profiles<u>.</u> ~~of:~~ S4-TIR products (red lines), S5-TIR products (blue lines) S4-UV products (red lines) and FUS product (dark red line). In each panel, while <u>the</u> solid dark red line is a single one, <u>the</u> red and green lines are both 55 overlapped lines<u>,</u> and <u>the</u> blue lines are <u>eight</u>~~8~~ overlapped lines (one for each L2 product).

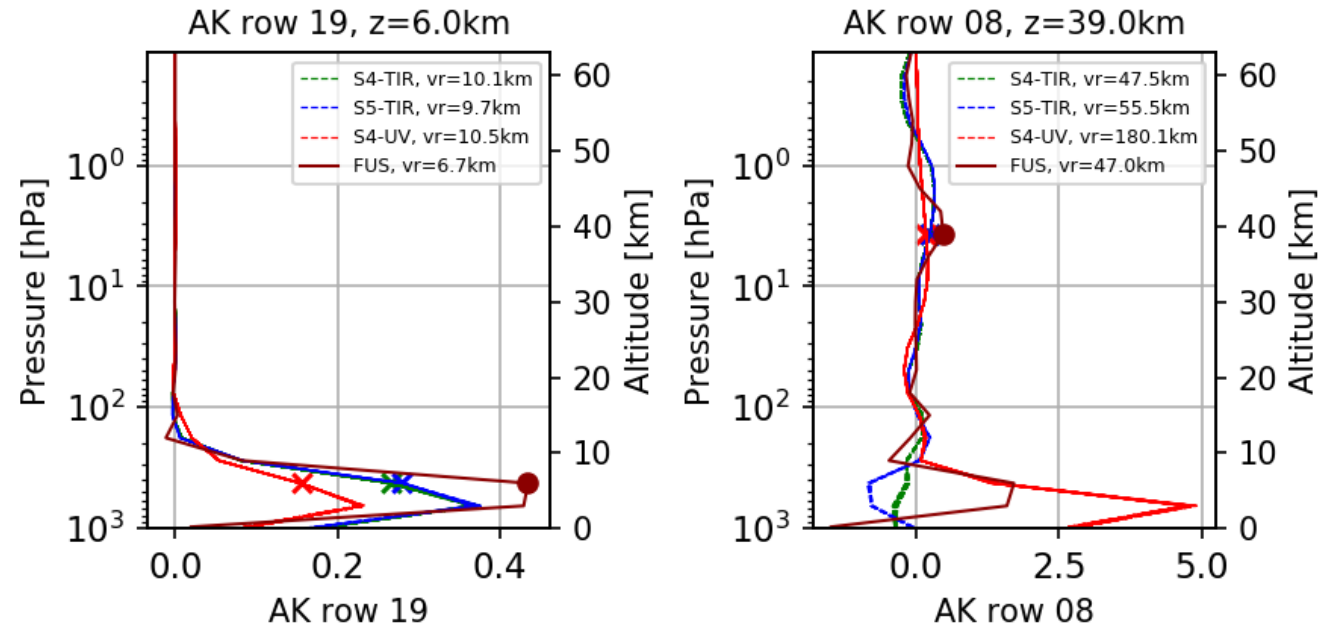

Figure 4 (Left panel): Rows of AK matrices at 6 km. (Right panel): Rows of AK matrices at 39 km S4-TIR products (red lines), S5-TIR products (blue lines) S4-UV products (red lines) and FUS product (dark red line).

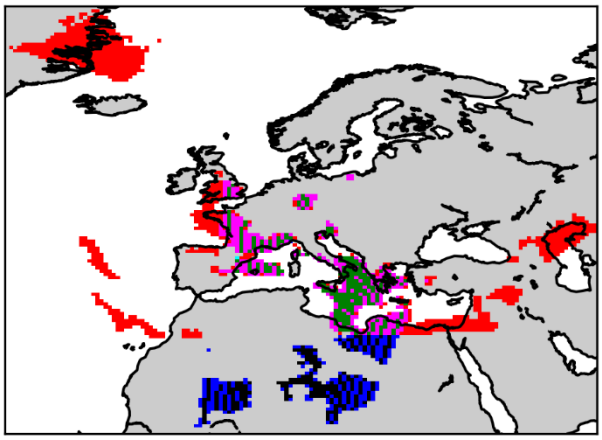

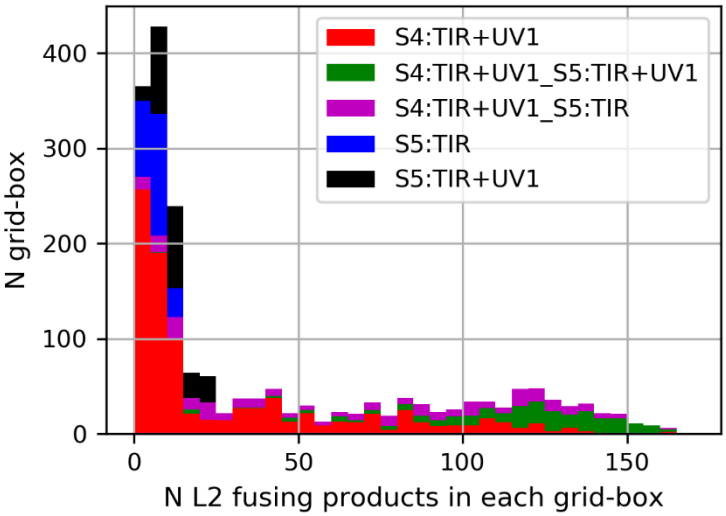

Figure 5. Left panel: geographical distribution of FUS products differentiated by FUS type where the effect of the lower resolution of S5-UV1 respect to the other L2 products is the cause of the periodic FUS type transitions in the Mediterranean area. Right panel: histogram of the number of cells with a given number of L2 measurements differentiated by FUS type.

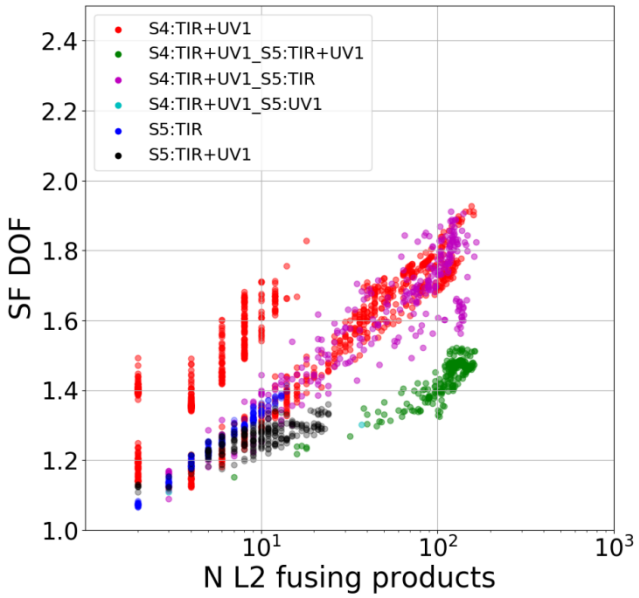

Figure 6: scatter plot of SF DOF as a function of the number of L2 measurements fused in each coincidence grid cell; different colours represent different FUS types.

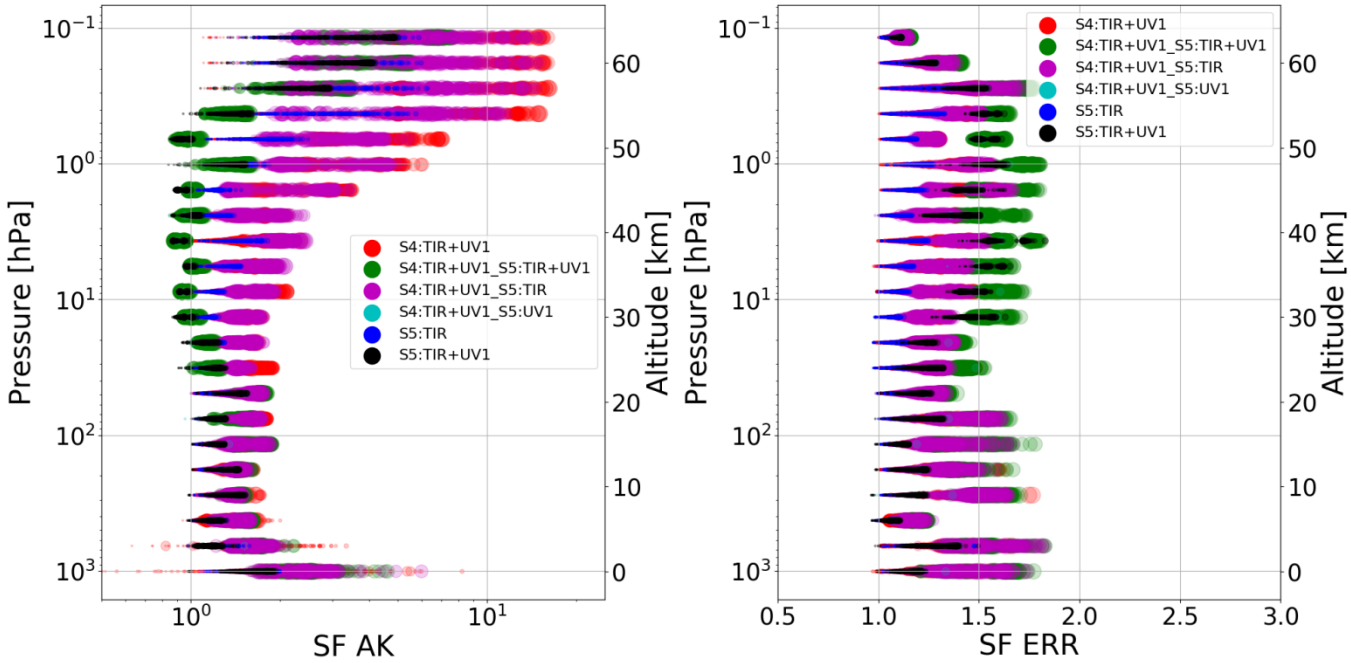

Figure 7 (Left panel): SF AK versus vertical level. (Right panel): SF ERR versus vertical level. In both panels, different colours of the symbols represent the FUS type, different sizes of the symbols represent the number of measurements that have been fused. The maximum symbol size shown in the legend corresponds to N=160.

545